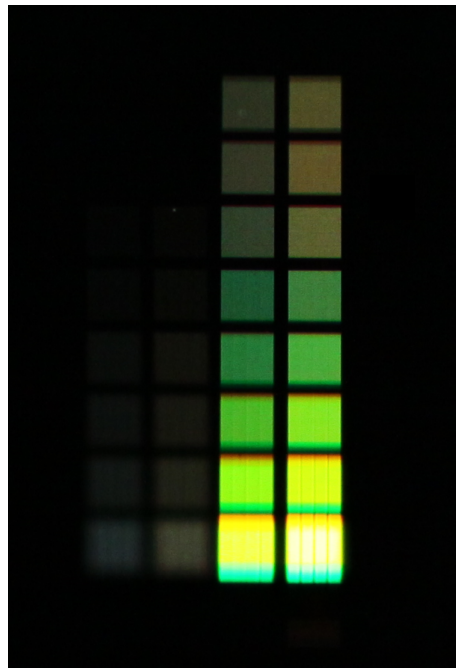# Plasmonics in metal hole arrays

C.B.Smiet

August 9, 2010

Quantum Optics and Quantum Information group
Supervised by:
Frerik van Beijnum
Martin van Exter
In collaboration with:
Chris Retif

Contents

1 Introduction

The phenomenon of the Extraordinary Optical Transmission (EOT) of metal-hole arrays was discovered by Thomas W. Ebbesen in 1998. Ebbesen wanted to study single-molecule spectroscopy. To that end he had fabricated a metal film with millions of tiny holes arranged in a regular array. In these holes the molecules to be studied would be placed. When this sample was held to the light, he could see light coming through it with the naked eye. This was unexpected, as the size of the holes was smaller than the wavelength of the light that passed through . The transmission of such an array was supposed to reflect the transmission of a single hole, which Bethe had theoretically calculated to be significantly magnitude smaller [1], [2]. Ebbesen set out to characterize this transmission with a spectrometer, and found that the transmission varies with wavelength, and showed transmission dips and peaks at frequencies related to the spacing of the holes. [3]

The extraordinary optical transmission was first attributed to surface plasmon resonances by Ebbesen [1]. Surface Plasmon Polaritons (SPP) are traveling electromagnetic excitations of a metal-dielectric interface. Later this was put up for discussion and a model using evanescent waves was proposed by Lezec [4]. In 2008 Philippe Lalanne entered the debate with a model that incorporates both a SPP component and a evanescent wave component.

The ability to send light through tiny holes and understanding how it interacts with structures will help advancement of technology in the field of nanophotonics. A sound understanding of light with nanostructures will help advance this field further.

In this thesis we try to quantify the contributions of SPPs and evanescent waves to the EOT experimentally and compare the results with the microscopic theory proposed by Philippe Lalanne in 2008. We are the first to experimentally test this theory. Measurements were made of two different samples, each containing may hole configurations. We study the transmission of hole arrays and random configurations of holes. In the chapter Methods and Materials we discuss the setup and samples used. We discuss the results obtained from the random configurations, arrays in the first sample, and arrays in the second sample in separate chapters. Briefly we take a look at the transmission of a hole array between crossed polarizers in the chapter crossed polarizers.

2 Theory

In this chapter we discuss the theory behind extraordinary optical transmission. We describe the SPP phenomenon, and discuss the theory proposed by Philippe Lalanne in 2008. We also discuss the theory behind the transmission of random hole arrays.

2.1 Surface Plasmon Polaritons

In a SPP the electromagnetic field of the incoming light interacts strongly with the free electrons in the metal. This leads to a propagating mode localized on the metal-dielectric interface. Due to the interaction with electrons momentum k_{spp} of a SPP is larger than that of freely propagating light. The momentum of a SPP is:

$$k_{spp} = k_0 \sqrt{\frac{\epsilon_d \epsilon_g}{\epsilon_d + \epsilon_g}} \tag{1}$$

where k_0 is the momentum of free light, and ϵ_d and ϵ_g are the dielectric constants of the dielectric and the gold respectively [5].

If you have a hole in a metal film, there will be a small fraction of the light that is transmitted directly, even though the hole is smaller than the wavelength of the light. Bethe has calculated the intensity of the transmitted light through a sub wavelength hole. The wavelength dependence of the transmission was found to be λ^{-4} [2].

A structure, like a hole or a corrugation on the surface can scatter the incoming light parallel to the surface into a plasmon mode. The loss that a plasmon experiences is dependent on the properties of the metal, and varies for different frequencies. For gold plasmon loss becomes large below 700 nm wavelength of light. By applying polarized light, one can control the direction in which the SPPs are exited. If one applies horizontally polarized light, then plasmons cannot be exited that travel in the vertical direction, and the same for vertically polarized light.

2.2 Microscopic Theory of the EOT

If holes are placed in a regular structure then certain frequencies of light excite plasmons that fit into a resonant mode of the array. These plasmons travel over the surface of the metal, before traveling through the holes and contributing to the transmission of the array. The light that exits the plasmon resonant mode has picked up a wavelength dependent phase delay, and interferes with the light that was directly transmitted through the holes. At some frequencies this interference is constructive, and at other frequencies it

is destructive. This causes a distinctive asymmetric Fano [6] lineshape in the transmission spectrum.

In 2008 Philippe Lalanne proposed a new model for the EOT. He set up a model that involves only plasmons and direct transmission, and compared that with computer simulations. In this model the transmission of the fields through a metal hole array taking only plasmons into account is:

$$t_a = t + \frac{2\alpha\beta}{u^{-1} - (\rho + \tau)} \tag{2}$$

Here t is the direct transmission through the hole array. α and β are the in- and outcoupling coefficiënts the light to the plasmon mode at a row of holes. $u^{-1} = e^{\pm i k_{spp} a_0}$ is the phase delay accumulated by the SPP over a grating period a_0. ρ and τ are respectively the reflection and transmission coefficiënts of a plasmon traveling over the gold surface and encountering a row of holes. All these quantities are complex, representing both amplitude and phase.

Using this model, Lalanne has shown that the transmission of a array is only attributable to SPPs for roughly 50%. The difference between the plasmon-only model and the observed transmission is ascribed to another effect which he calls the Cylindrical Wave (CW). Figure 1 shows the decomposition of the surface field into a CW and a SPP mode. This CW attenuates faster than the SPPs. The momentum of the CW travels is k_0.

The fact that the CW travels less far than plasmons gives us an experimental way to verify the microscopic theory of the extraordinary optical transmission, and to separate the effects of the SPP resonance and the CW contribution to the extraordinary optical transmission. We have fabricated arrays in which the horizontal distance between the holes has been varied, in integer multiples of a basic lattice length a_0. The vertical distance between holes is kept constant at $1a_0$. By applying horizontally polarized light, we can look at the transmission caused by plasmons traveling in the horizontal direction. For the arrays where the horizontal distance is small, the CW will contribute to the extraordinary optical transmission, but after a while the horizontal spacing becomes so large that only the SPP effect causes the transmission.

We can use the plasmon-only model to fit the arrays with large horizontal spacing. This model has many independent variables, and that makes fitting problematic. By fitting not only one spectrum, but many spectra with different spacings, the accuracy of the fit can be improved. This is possible because all the different arrays will have a resonance at the same wavelength. Here the coefficiënts will be the same for all the different arrays. The obtained co-
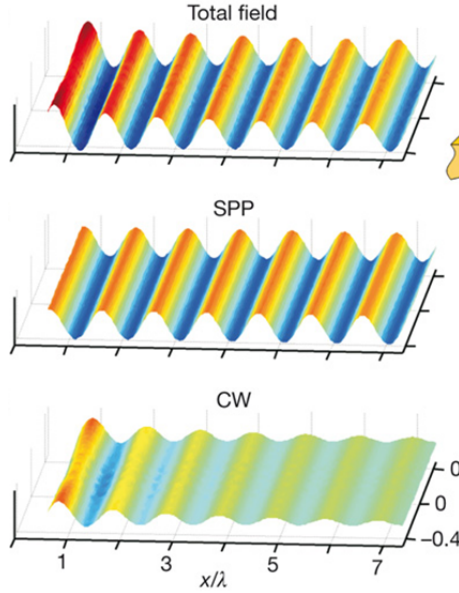
Figure 1: The field on a surface decomposed into the SPP contribution and the cylindrical wave contribution. The cylindrical wave attenuates faster than the surface plasmon. Image from Lalanne's nature paper [7].

efficiënts can be used to make a prediction for the plasmon-only transmission of arrays with small horizontal spacing, and quantify the CW contribution.

2.3   Scaling of the Transmission of Hole Arrays

If light is reflected from or transmitted through a periodic structure, the structure will automatically act as a grating. This means that reflected or transmitted light is diffracted into different orders at different angles. The equation for the angles of diffraction of a periodic structure with period na_0 is [8]:

$$\sin(\theta_q) = \sin(\theta_i) + \frac{\lambda \cdot q}{n \cdot a_0} \tag{3}$$

where θ_i is the angle of incidence, which is zero for normal incidence. λ is the wavelength, and q any integer for which a solution exists. For larger n there will be more orders visible.

If we want to measure the total light transmitted through a periodic array per hole we first have to divide by the density of holes. This density scales as n^{-1}, so dividing by density, we multiply with n.

6

Secondly we have to take into account that if the distance between the structures increases, there will be more diffraction orders, and less light in the zeroth order transmission spectrum. If we measure only the zeroth order transmission, we have to take this into account. The intensity of light in the zeroth order transmission is inversely proportional to the horizontal spacing, and thus to n. Compensating for this adds another factor of n. If we want to scale the different arrays to the transmission per hole, we must thus multiply by n^2

This argument assumes that the amount of light scattered from a single hole is equal for all directions. This also implies discontinuous jumps in the transmission at frequencies where new orders appear (Wood anomalies) [9]. These jumps are not observed.

2.4   Random Hole Configurations

A random hole configuration is, as the name suggest, a configuration where the holes are positioned randomly. If light is shone on such a configuration, plasmons that travel over the surface are still created, but there is no periodic structure into which some plasmons fit better than others. Plasmons still assist in the transmission of the array, but they do not cause a Fano transmission peak.

The measured transmission of such a random hole configuration should shows the direct transmission of light through the holes in addition to the effect caused by plasmon-assisted transmission. The magnitude of this effect is unknown. The plasmon-assisted transmission is proportional to the loss plasmons encounter when traveling over the surface. This loss is wavelength dependent, and for gold the loss is large for wavelengths below 700 nm. Above 700 nm the plasmon loss gradually settles [10].

The transmission spectrum of a random hole configuration could thus show the changing plasmon loss around 700 nm, but for larger hole separations the functional form will become equal to the transmission of a single hole.

Because of the lack of structure in a random The transmitted light will scatter in all directions, for all arrays. The transmission per hole should be proportional to hole density.

3 Methods and Materials

In this section we discuss the experimental setup, the measurement method and the samples.

3.1 setup
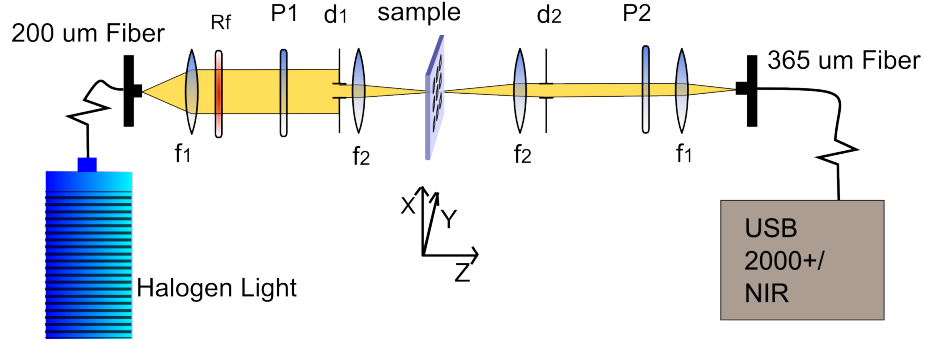
Figure 2: The setup used for the experiments. A Halogen light shines light through a fiber. This light is collimated by lens (f_1), passes through a filter (Rf) polarizer (P_1), and aperture (d_1). A sharp image of the fiber is created on the sample by lens (f_2). The transmitted light is collimated. The aperture (d_2) and polarizer (P_2) are only in place for some experiments. The light is imaged into a fiber and transmitted to the spectrometer.

The setup used in this experiment can be seen in figure 2. A 24 V halogen light (Ocean Optics HL 2000 FHSA) creates the white light used. We couple this light into a 200 μm fiber. The divergent beam exiting the fiber is collimated by the first lens (f_1=50 mm), and passes through a redfilter (RF), polarizer (P1), and an adjustable aperture (d_1). The second lens (f_2=75mm) makes a 1.5 times magnified sharp image of the fiber exit on the sample. The light that passes through the sample is collimated again by a lens (f_2). (there is an optional aperture d_2 and polarizer P2). The light is finally imaged into a 365 μm fiber that leads to the USB2000+spectrometer. The sample is mounted on a translation stage with freedom to move in the X, Y and Z direction. This makes it possible to change the location of the image of the fiber on the sample.

Two spectrometers were used for this experiment. For most of the measurements the Ocean Optics USB 2000+ spectrometer was used. This is a Miniature Fiber Optic Spectrometer. It has a 2048 element detector and is designed to measure light from 506 to 1170 nm. For other measurements the Ocean Optics NIR 512 spectrometer was used. This fiber spectrometer measures infrared light using a InGaAs detector, for wavelengths from 850 to 1713 nm. Data acquisition is done with Ocean Optics proprietary Spectra Suite software.

The RG610 redfilter filters out light below 610 nm. This filter is placed because the grating of the USB2000+ spectrometer has some light in the second diffraction order. This means for example that light of 550 nm can end up on the 1100 nm pixel, and create false signal.

Spectrometers suffer from nonlinearity issues. Effectively the signal measured is not linear with the amount of light falling on the detector. For us it is important to compare the relative intensities of different arrays.

The Ocean Optics USB200+ spectrometer has a nonlinearity correction function. The nonlinearity is measured and fitted with a function of 7 variables. The pixel values of the obtained spectra are multiplied by this function to obtain the corrected light intensity per pixel.

It is important to note that the Ocean Optics NIR 512 spectrometer does not have a nonlinearity correction function.

3.2 Transmission Measurement

For measuring the transmission you have to compare the signal of the lamp with the much weaker signal of light that passes through the holes. Higher accuracy in transmission measurements can be obtained if the weak signal is measured at a longer integration time.

A CCD-based spectrometer with bias and dark current. Bias is a constant offset of the readout of the detector and dark current is signal that the CCD produces even though no light falls on the detector. Together this gives a time-dependent zero signal that must be subtracted from the spectrum before comparing. The transmission of the hole configurations were calculated in the following way:

$$T = \frac{I_{sample} - I_{samplezero}}{I_{ref} - I_{refzero}} \tag{4}$$

In this equation I_{ref} is the spectrum measured shining the light through the setup without the sample present. I_{sample} is the light passing through the sample. The two dark scans $I_{refzero}$ and $I_{samplezero}$ are taken by blocking the

path of the light and integrating the same time as the reference scan or the sample scan respectively.

3.3   Sample Design

Two different samples were created for this experiment. We will discuss the different sample designs in this section.

3.3.1   First Sample
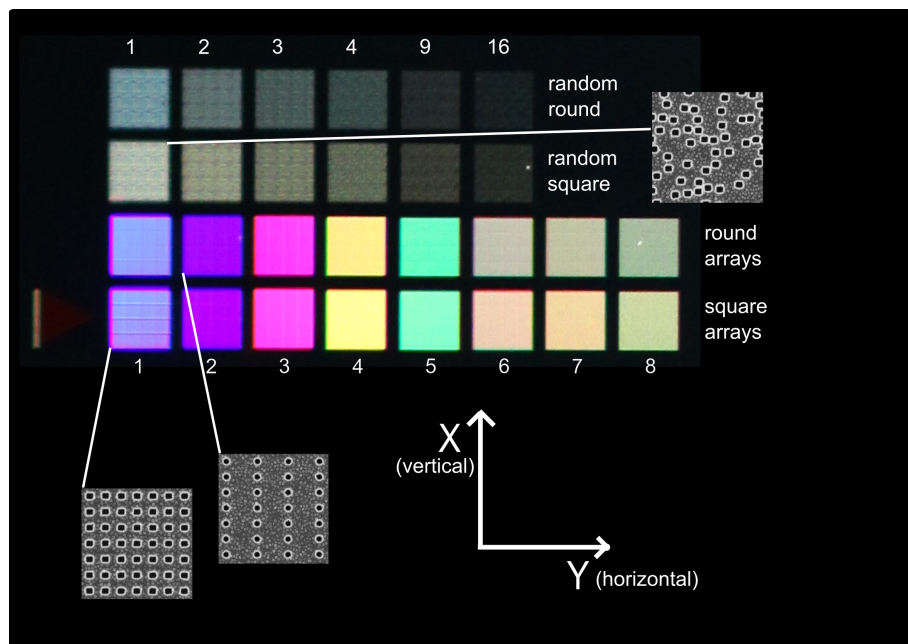
Figure 3: The first sample. The colored structures are 400 by 400 micron. This image is taken with a DSLR camera using a macro lens. Colors are as they appear to the eye. As the structures in the metal are very periodic, the light is diffracted in the same way as from a grating. A bright light is shone from the side, and the colors are caused by the different samples reflecting different colors in different directions.

The first sample can be seen in figure 3. The structures are 400 by 400 micron, and each square is a different hole configuration. The total thickness is roughly 222 nm. It consists of a 200 nm layer of gold with a 20 nm chrome layer on top. This is attached to a glass substrate by a titanium adhesion layer expected to be 2 nm. The thickness of the adhesion layer cannot be known for sure.

In figure 3 the upper two (grey) rows of squares that can be seen are the random configurations. The first row has round holes, and the second row has square holes. The average sample area per hole is respectively 1, 2, 3, 4, 9 and 16 a_0^2. The intensity of the light diminishes as the density of holes decreases. The locations of the random holes are generated by a Matlab script, and they are the same for the square and the round holes, but different for different densities. In the first four random configurations the hole density is the same as in the first four ordered arrays.

The lower two colored rows of squares are the ordered arrays. In the upper row the holes are round, in the lower row they are square. In the leftmost samples the horizontal distance between the holes is $1a_0$, and ascending in integer steps up to $8a_0$ spacing for the arrays at the far right.

Due to the writing method the square holes of the first sample are rectangular and the round holes elliptical. The square holes aren't perfectly square, but are elongated in the horizontal direction. The dimension of the square holes is 170×150 nm. The round holes have a diameter of 140 nm. A SEM-image of the holes can be seen in the inset in figure 3

There is a hole (a large, unintended one) in the $1a_0$ random round configuration (upper left in figure 3). Because of this the transmission spectra of this configuration were not considered.

3.3.2 Second Sample

The second sample is thinner than the first sample. The gold layer is only 170nm, with 20 nm of chrome on top. It was possible to produce this sample without a titanium adhesion layer on the glass, so the plasmons will encounter less resistance when traveling over the glass/gold interface.

The layout of the second sample is very similar to the first, but the amount of arrays have been expanded. This sample contains 52 configurations. The round and square arrays have both been expanded to $10\ a_0$, and complemented with 12, 14, 16 and 18 a_0. The random configurations have been added on with configurations where the area per hole is 25, 36, 81, 144, 225, and 400 a_0^2.

The holes in the arrays are larger in this second sample. These square holes are now square, 175×175 nm, and the round holes measure 165 nm diameter. In the random configurations the holes are still exactly the same as in the first sample.

3.4   Sample Characterization

The distance between the holes in the ordered arrays in the horizontal direction is an integer times 450 nm. The accuracy of this spacing was investigated by looking at the angle of first-order reflection of red 635 nm laser light in the even arrays.

Using equation 2.3 we can see that equation for the angles of reflection in our sample n at normal incidence is:

$$\theta_q = \arcsin(\frac{\lambda \cdot q}{a_0 \cdot n}) \tag{5}$$

For all samples with even n, there is a solution to this equation where $\frac{q}{n} = \frac{1}{2}$. Filling in the values for $a_0 = 450$ and $\lambda = 635$nm, all the samples with even n have light exiting at an angle of 44.9°.

We shine this light on a CCD to accurately measure the displacement of this spot when different arrays are illuminated. The displacement was less than 90 μm after propagating 8 cm, so we can conclude that the differences in the horizontal spacing between arrays must be less than 0.5 nm.

4   Random Configurations

We measured the transmission spectra of all the random configurations in the first and second samples. If only one type of holes is discussed, the transmission of round and square holes are similar. Surprising differences between the configurations in the first and second sample were observed.
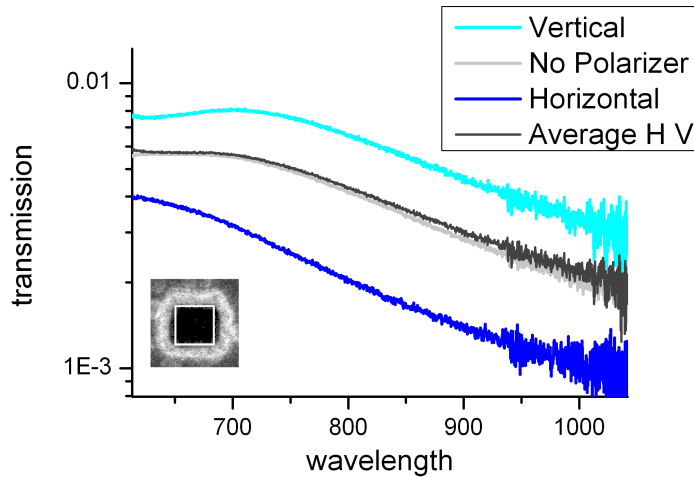
4.1   Random holes in the First Sample
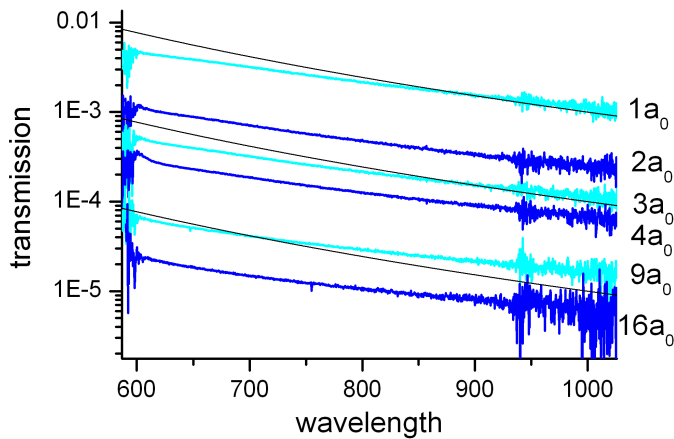
Figure 4: The transmission spectra of the random square arrays. The black lines follow Bethe decay (λ^{-4}). It is clear that these arrays do not follow this functional form

The transmission spectra of the random square configurations can be seen in figure 4. The transmission for the random round arrays are the same. The transmission of these spectra do not follow the pattern predicted by Bethe [2]. The black lines are arbitrarily plotted, and fall off as λ^{-4}. The transmission spectra of our samples fall off less rapidly.

The transmission spectra were fitted with a function of the form $a\lambda^{-b}$, to find the values for the coëfficient b. The different arrays have similar values for the coëfficient b. For the square configurations (pictured in figure 4) this value lies between 2.68 and 2.97. For the round configurations this value lies between 2.71 and 3.47.

In figure 5 you can see the transmission spectra of the first random square configuration for different incoming polarizations. The density here is 1 hole per $1a_0^2$ area, the same density as the first array. The horizontal polarization

Figure 5: The transmission of the densest random square configuration in the first sample for three different polarizations. The inset shows a SEM image of a single hole. The white square is perfectly square. You can see that the hole is rectangular.

has a lower transmission than the vertical polarization, and there is also a peak in the transmission around 700 nm. The average of the horizontal and vertical polarization was calculated, and found out to be equal to the transmission without polarizers.

We hypothesize that this effect is caused by the fact that holes are wider in the horizontal direction. Plasmons are exited more effectively from a hole perpendicular to the long axis [11]. Plasmons coming from light with a wavelength below 700 nm experience large loss when traveling over a gold interface, so the transmission of the hole array drops down below 700 nm. Above 700 nm the loss experienced becomes more or less constant, and the transmission of the configuration becomes similar to the transmission of a single hole.

In the time of measuring there has been a change in the transmission spectra of the random configurations. Especially the densest random square configuration was affected. The early spectrum can be seen in 4. The horizontal polarization in figure 5 shows the changed spectrum. The overall transmission has become a little lower, and a 'bend' in the transmission has appeared around 700 nm. The maximum change is less than 10%, and at 700 nm the transmission is the same. A possible explanation could be aging and pollution of the sample, which would lower transmission, combined with settling and crystalizing of the gold, which would enhance the plasmon-action,

and make the bend in the spectrum appear.

4.2   Random holes in the Second Sample
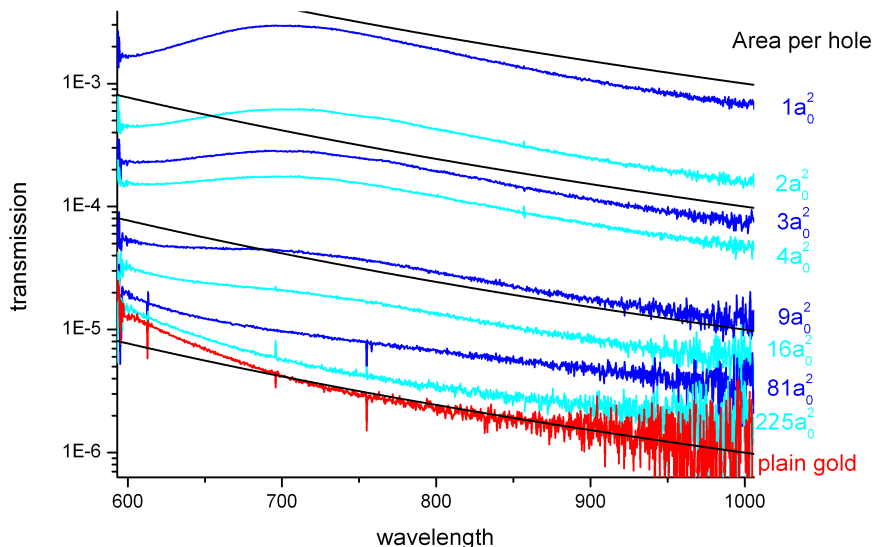
Figure 6: The transmission spectra of the random round arrays in the second sample. The red line is the transmission of only the gold. The black lines follow Bethe decay.

The second sample has many more random configurations. In figure 6 the transmissions of all the random round configurations can be seen. The transmission of the random square arrays follow the same pattern. In the last few arrays the hole density becomes so low that the transmission approaches that of just the plain gold. The random configurations in the second sample now do follow the decay predicted by Bethe. As the average distance between the holes increases you can also see the peak at 700 nm decrease, and the transmission starting to approach the transmission of plain gold.

In comparison with the first sample there is more structure to be seen, notably a peak at 700 nm. We attribute this peak to plasmon assisted transmission through the random array (which becomes lower below 700 nm). The peak at 700 nm in the random transmission becomes less prominent if the spacing between the holes is larger.

15
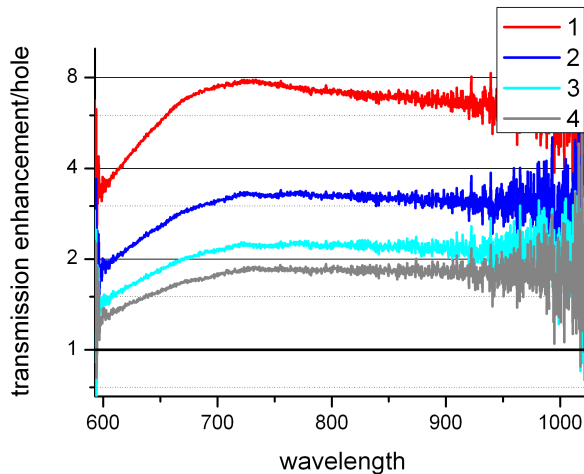
Figure 7: Enhanced optical transmission of random hole configurations. In this figure the enhanced transmission per hole of the first four random configurations (density:1 hole per 1-4 a_0^2) with respect to the transmission of the fifth (density: 1 hole per $9a_0^2$). The transmission of the first configuration is about 7 times higher for frequencies above 700 nm
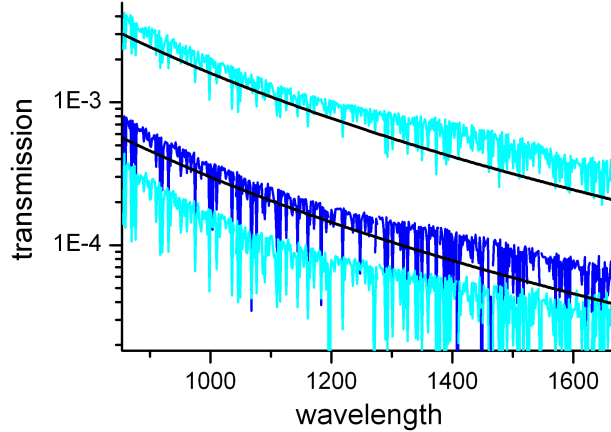
The transmission of the first random configuration is much larger than the others, as can be seen in figure 6. The transmission per hole is also larger. This transmission per hole is calculated by dividing by hole density. We want to quantify this enhancement of the transmission. We want to divide the transmission of the first few configurations with the transmission of a configuration where this enhancement is gone. We can only do this if the transmission through the holes is much larger than the transmission of the gold. That is not true for the last few random configurations.

The transmission for the fifth configuration, where the density is 1 hole per 9 a_0^2, is significantly larger than the transmission of the gold (5-12 times). The enhanced transmission is not gone yet, but it is significantly smaller than for the first four samples, where the density is 1 hole per 1-4 a_0^2 respectively. We divide the transmission per hole of the first four random configurations by the transmission per hole of the fifth to give an indication of the enhancement of the transmission. As the fifth configuration still has enhanced transmission itself, the true enhancement will probably be even larger.

in figure 7 the enhancement in transmission can be seen. We can clearly see an enhanced optical transmission of random hole arrays at high hole densities. This enhancement is constant at optical wavelengths above 700 nm, and reduces for wavelengths below 700 nm. We hypothesize that this

16

enhancement is caused by non-resonant surface plasmons traveling over the surface.

Figure 8: The transmission of the first three random square samples in the near infrared region. The black lines have the same functional form as Bethe.

In figure 8 the transmission of the first three square random configurations are plotted. The transmission spectra obtained using the NIR 512 spectrometer are a lot noisier. This spectrometer also has no nonlinearity correction. In the near infrared region the transmission of the random configurations in the new sample follow the functional form predicted by Bethe as well.

The frequencies measured by the two spectrometers overlap between 800 and 1050 nm. The spectrum measured with the USB 2000+ spectrometer is 30-50 % higher in this overlap region. We believe that the functional form measured in the near infrared is correct, but that this difference is caused by nonlinearity in the NIR-512 detector.

Overall we can conclude that the functional form of the transmission of random holes is strongly dependent on sample thickness and plasmon losses. Therefore it's hard to be conclusive on the direct transmission.

5 Hole Arrays in the First Sample

The transmission of the hole arrays in the first sample was not as high as expected. The effect of plasmons was hard to see.
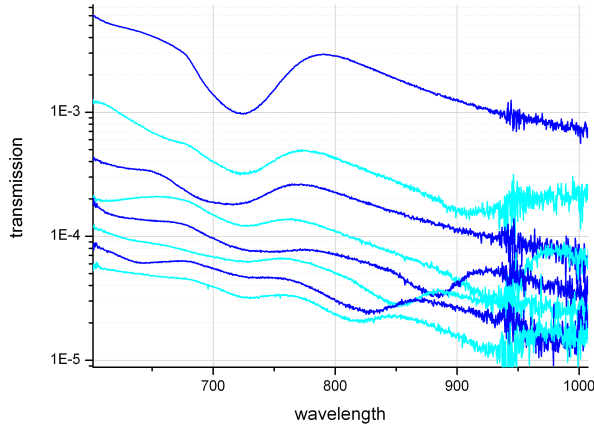
5.1 Transmission Spectra

The transmission of the hole arrays show the Fano resonance shape. In figure 9 you can see the transmission of the $1a_0$ square array compared with the transmission of the random square array of the same density. The transmission of the arrays is a perturbation on the transmission of the random configuration, and as you can see, not a very strong one. The transmission of the array at the maximum of the Fano peak is about 0.5 %. Because of the thickness of the metal and the presence of the Ti adhesion layer, and the small size of the holes, the plasmon resonance is not as large as expected.
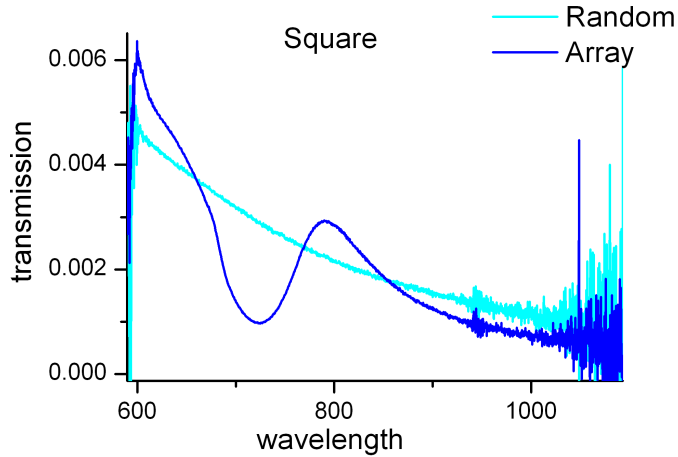
Figure 9: Comparison between the transmission of the $1a_0$ square array and the random array with the same hole density.

The transmissions of the square arrays in the first sample can be seen in figure 10. The transmission spectra of the round arrays are similar to those of the square arrays. The resonances are too weak to fit the plasmon-model to. All the arrays exhibit a dip at about 725 nm, where the fundamental resonance on the glass-side is expected.
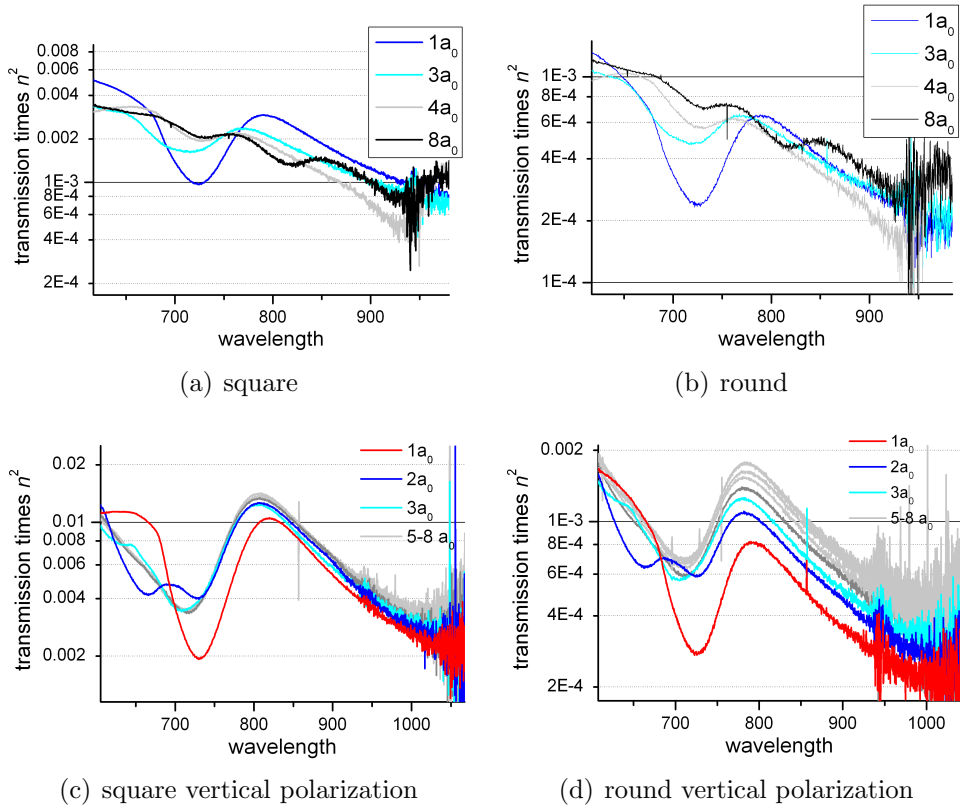
Figure 10: The transmission spectra of the square arrays. Horizontal hole distance ranging from $1a_0$(highest transmission) to $8a_0$ (lowest transmission).

5.2   Analysis

We also measured the light transmitted through the hole arrays with the incoming polarization in the vertical direction. This means that the plasmons travel through the columns of holes, and that the distance to the next hole is always $1a_0$. The scaling to determine the transmission per hole is also valid for vertical polarization. in figure 11 (a) (b) the transmission per hole with vertical polarization is shown.

In figure 11 (c) and (d) the scaled transmission of the square arrays with vertical polarization is shown. scaling is done by multiplying by n^2. Here plasmons do not travel in the horizontal direction. For close horizontal spacing you expect to see some effect of the adjacent rows of holes and the (1,1) resonance. If the horizontal spacing between the rows becomes large, vertically traveling plasmons will effectively be the only contribution to the transmission. For large horizontal separations and vertical polarization the transmission per hole becomes constant. In figure (c) the spectra of the 3 through 8 a_0 arrays lie right on top of each other. We can conclude that scaling with n^2 works for the square arrays. in figure (d) you can see that the scaling works less well for arrays with round holes.

(a) square

(b) round

(c) square vertical polarization

(d) round vertical polarization

Figure 11: Scaling. (a) and (b) show the normalized transmission of the square and round arrays with horizontal polarization. (d) and (c) show the transmission per hole of the arrays with horizontal polarization. If the scaling works, the 5-8 spectra should lie on top of each other. The scaling works well for the square arrays, not as well for the round.

.

6 Hole Arrays Second Sample

The transmission of the hole arrays in the second sample are a lot higher, and the features are more pronounced than in the first sample.

6.1 Transmission Spectra

(a) new sample   (b) old sample
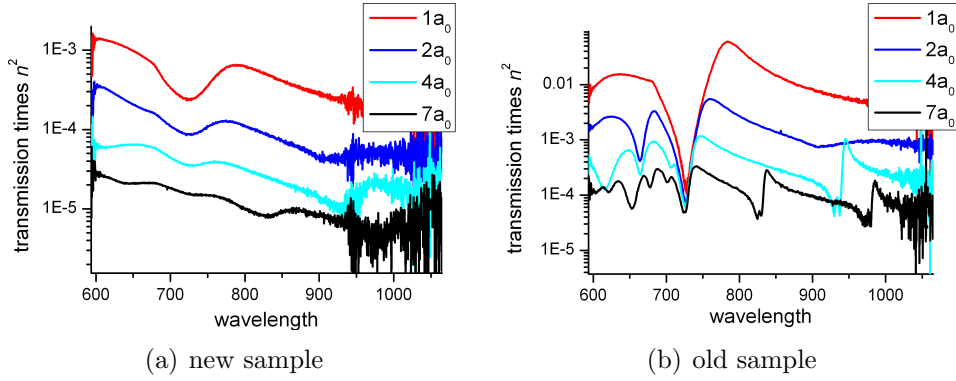
Figure 12: The transmission spectra of the second sample round arrays in (a) and the first sample round arrays in (b). all the features that are visible in (a) are also visible in (b), but they are a lot less pronounced.

Luckily the transmission spectrum of the arrays in the second sample show the strong asymmetric Fano resonance that signifies the EOT. The maximum transmission of the square hole arrays is 12,5-14% at the peak of the Fano resonance. For the round hole arrays the maximum transmission is 7,5%. In figure 12 you can see the transmission of the square arrays in the new sample compared with the square arrays in the old sample. All the resonances are still in the same positions. Where the $7a_0$ array in the new sample has three distinct clear resonances, these are only seen as slight wiggles in the old sample. The transmission spectra of the round arrays have the same features as the square arrays, but the transmission is about half as high.

In the transmission spectra of the arrays with horizontal spacing larger than $4a_0$ a second Fano resonance becomes visible in the spectral range that we are looking at. The dip in these Fano resonances is split in two. The cause of this effect was found to be spread in incoming angle. decreasing the aperture of the incoming light (aperture d_1 in figure 3) decreases the angular spread of the incoming light, and decreases the split of this dip. Unfortunately decreasing the aperture diameter comes at the price of reduced light intensity and increased integration time.

The transmission spectra clearly show that the minimum of the Fano peak stays at the same spot. The peak of the Fano transmission is not constant at all, and is in a different position for all the samples. This suggests that the position of the dip in the transmission is a much more fundamental aspect of the interaction of light with metal hole arrays than the peak (which is what the research up to now has been paying most attention to).
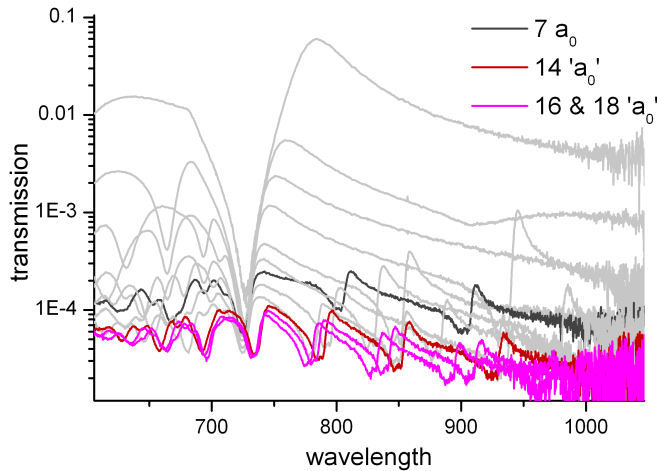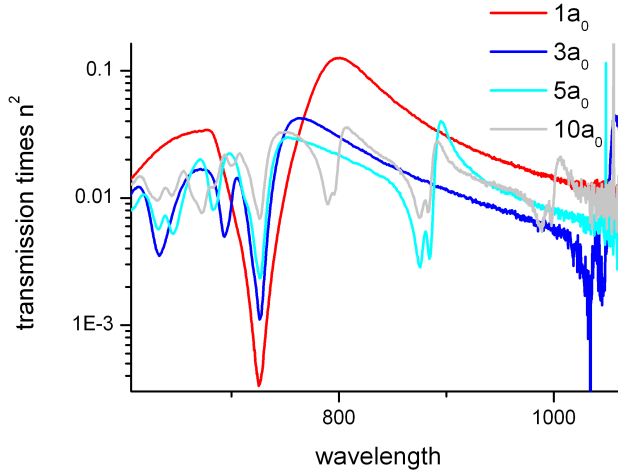

Figure 13: Transmission of the round arrays. The last three red arrays do not share the dip in transmission at 725 nm that all the other arrays show. The dark $7a_0$ array should also have resonances in the same location as the darker red $14a_0$ array, but it doesn't. This prompts us to believe that the horizontal spacing between the last three arrays is not an integer multiple of a_0

There were some problems with these samples. In figure 13 the troubled spectra are highlighted. There is a problem with the last three arrays. We hypothesize that the holes are not an integer times a_0 apart. This can be seen because the dip present in all other arrays at 725 nm is shifted to the red. the $14a_0$ array (dark red) should also have resonances at the same wavelength as the $7a_0$ sample (dark grey), but this is not the case.

6.2 Analysis

The scaling argument used for the old samples is of course also applicable for the new samples. in figure 14 you can see the 1, 3, 5 and 10 a_0 arrays normalized in this way. The plasmon resonance is of course the sharpest in the $1a_0$ array, both the dip and the peak are more pronounced. The round arrays scale with n^2 as well in the new samples. The normalized peak transmission

Figure 14: The transmission of the square hole arrays normalized to transmission per hole. the resonance of the $1a_0$ array is the largest of all.

of the 3, 5, and 10 a_0 arrays are about the same, but the peak transmission of the $1a_0$ sample is more than double as high.

Lalanne's plasmon-only model was also used to fit these samples. in figure 15 you can see the result of this fitting. The colored lines referred to in the legend are the measured transmission spectra of the round arrays, and the red lines are the result of fitting to these spectra. The arrays 2 through 7 a_0 have been fitted simultaneously, using the same parameters. The model can explain the features in all the arrays. In 5, 6, and $7a_0$ a second Fano peak has entered the fitting regime. You can see that the model accurately accounts fore these resonances, but cannot incorporate the splitting of the dip. This is because the model assumes normal incidence of the light, and the splitting of this dip is caused by angular spread. Reducing this split can make the fits more accurate.

If our model is correct the parameters obtained from fitting arrays 2 through 7 predict the plasmon-only contribution of the extraordinary transmission. Using these parameters we can also calculate the transmission predicted for the $1a_0$ array caused only by the plasmons. in figure 15 the blue line is the transmission of the $1a_0$ array, and the red line below that is the predicted transmission using the model. The scale is logarithmic, so they look quite close, but in fact the peak intensity predicted by the plasmon-only model is half that of the measured transmission.
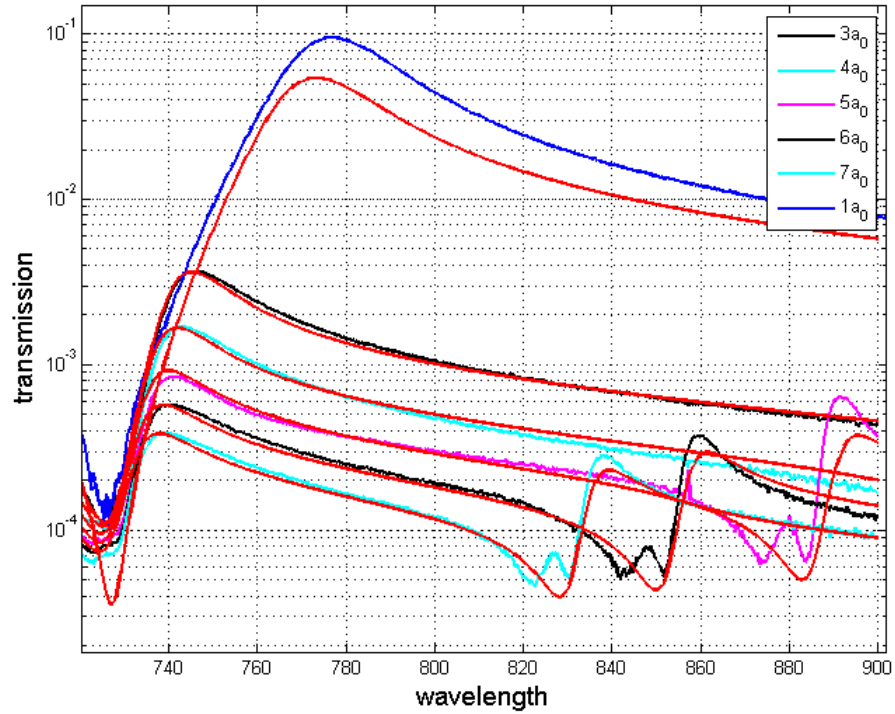
Figure 15: Fitting Lalanne's plasmon model to the array. The arrays 2 through 7 a_0 have been fitted with the model. The parameters obtained from this fit are used to generate the curve that resembles the $1a0$ transmission. This curve is lower than the measured transmission for the $1a0$ array.

.

7   Crossed Polarizers

In our research we have also briefly experimented with measuring the depolarizing properties of the samples. The sample is placed between two polarizers that are rotated 90 degrees with respect to each other. The light is normally incident.
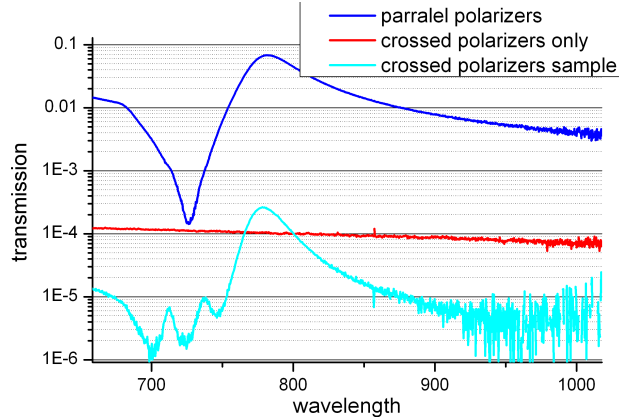
Figure 16: Round array between crossed polarizers. There is depolarization of the light at resonant frequencies and new structures seem to emerge.

One would expect to see the spectrum seen with parallel polarizers diminished by the blocking factor of the crossed polarizers. In figure 16 Instead new structure is visible in the transmission of the hole arrays. Between 750 and 800 nm the transmission of the sample between crossed polarizers is even larger than the transmission of the polarizers with nothing in between.

The transmission of only the crossed polarizers is very high. With polarizers you should be able to get an attenuation factor of 10^{-8}, in stead of the 10^{-4} observed. This could improve the measurements.

Further investigation into this phenomenon could prove interesting. The emerging structures seem to have a Lorentzian character, so the resonant frequency can easier be found from the spectra.

Similar measurements were simultaneously performed by Lubisja Babiç and Louwrens van Dellen on a 2d photonic AlGaAs crystal. Polarization turning at resonant frequencies at normal incidence were also observed. Transmission between crossed polarizers at off-normal incidence has been used to find the frequency of the resonant mode of photonic crystals.

8 Conclusion and Discussion

The conclusions drawn from this experiment can be grouped into three categories; random configurations, arrays and crossed polarizers.

Random Configurations The transmission of random hole configurations follow Bethe's predicted decay and fall off as λ^{-4} in the second sample, but do not in the first sample. This is also true for the second sample in the near-infrared region. The transmission of these arrays is strongly dependent on hole size, plasmon attenuation, and layer thickness.

The random hole configurations measured all have the same small hole sizes. It would be nice to measure the transmission of random holes with holes the same size as the holes in the arrays of the second sample. This could help in giving a prediction for the direct transmission through the larger holes, and assist in the fitting of the arrays.

We can see an enhanced optical transmission of random hole arrays. This enhancement is dependent on hole density. An enhancement of more than 7 times has been found.

Arrays We have investigated the effect of the extraordinary optical transmission and tried to verify Lalanne's microscopic theory of the extraordinary optical transmission. No conclusive statement can be made at the moment, but the gathered data shows the existence of another effect besides the plasmon resonance in the extraordinary optical transmission of metal hole arrays. More analysis is needed to further quantify this.

The resonant dip in the arrays is in the same position for all samples, but the maximum of the transmission peak varies per array. This is a strong indication that the dip in the resonance frequency is a more fundamental aspect of light in hole arrays than the position of the transmission peak.

Fitting Lalanne's plasmon-only model to the measured spectra works well. The model can take higher order resonances into account. Minimizing the splitting of the higher resonances could produce better fits.

Scaling the transmission spectra of the arrays by multiplying with n^2 works well. In the first sample it works better for the square arrays than for the round arrays, in the new arrays it works well for both.

Crossed Polarizers There is depolarization of the transmitted light at resonant frequencies. More investigation into this phenomenon could help in further analysis of the phenomenon of the EOT.

References

[1] Ebbesen, T. W., Lezec, H. J., Ghaemi, H. F., Thio, T. & Wolff, P. A. Extraordinary optical transmission through sub-wavelength hole arrays. Nature 391, 667-669 (1998)

[2] Bethe, H. A. Theory of diffraction by small holes. The Physical Review 66, (1944)

[3] Thio, T. A bright future for subwavelength light sources. American Scientist (Jan-Feb 2006)

[4] Lezec, H. J., Thio, T., Diffracted evanecent wave model for enhanced and surpressed optical transmission through subwavelength hole arrays. Optics Express(2004)

[5] Raether, H. Surface Plasmons on smooth and rough surfaces and on gratings. Springer-Verlag, Heldelberg, (1988).

[6] Fano, U. Effects of Configuration interaction on intensities and phase shifts. Physical Review 124, 18661878 (1961).

[7] Lalanne, P., Haitao, L. Microscopic theory of the extraordinary optical transmission. Nature 452, 728-731 (2008)

[8] Saleh, B. E. A., Teich, M. C. Fundamentals of Photonics, Wiley, (1991)

[9] Wood R. W., Anomalous diffraction gratings. Physical Review 48, 928 (1935)

[10] Maier, S. A., Plasmonics: fundamentals and applications. Springer (2007)

[11] van der Molen, K. L., Klein Koerkamp, K. J., Enoch, S., Segerink, F. B., van Hulst, N. F., Kuipers, L., Role of shape and localized resonances in extraordinary transmission through periodic arrays of subwavelength holes: Experiment and Theory. Phys. Rev. B 72, (2005)